Protection of Radial Circuits with High Penetration Distributed Photovoltaics

Thomas E. McDermott
Pacific Northwest National Laboratory
Richland, WA, USA
Thomas.McDermott@PNNL.gov

Sakis Meliopoulos
Georgia Tech
Atlanta, GA, USA
Sakis.M@GATech.edu

Meghana Ramesh
Pacific Northwest National Laboratory
Richland, WA, USA
Meghana.Ramesh@PNNL.gov

George Cokkinides
Georgia Tech
Atlanta, GA, USA
George.Cokkinides@ECE.GATech.edu

Jeff Doty
Pacific Northwest National Laboratory
Richland, WA, USA
Jeff.Doty@PNNL.gov

Jaime Kolln
Pacific Northwest National Laboratory
Richland, WA, USA
Jaime.Kolln@PNNL.gov

Neil Shepard
Oak Ridge National Laboratory
Chattanooga, TN, USA
ShepardNE@ORNL.gov

Gefei Kou
Dominion Energy Virginia
Richmond, VA, USA
Gefei.Kou@DominionEnergy.com

Francisco Velez
Dominion Energy Virginia
Richmond, VA, USA
Francisco.Velez@DominionEnergy.com

Ray Johnson
S&C Electric
Chattanooga, TN, USA
ray.johnson@SandC.com

David Duke
Chattanooga Electric Power Board
Chattanooga, TN, USA
DukeDA@EPB.net

Joshua Hambrick
Telos Energy
Chattanooga, TN, USA
Joshua.Hambrick@Telos.Energy

Rui Fan
University of Denver
Denver, CO, USA
Rui.Fan@DU.edu

***Abstract*—The paper addresses the shortcomings of distribution protection systems as distribution level photovoltaic installations as well as other inverter based distributed resources are added to the system. Several protection schemes have been evaluated, including distance-based, estimation-based and learning-based. The paper summarizes the results and provides recommendations.**

***Index Terms*—distance protection, radial distribution feeders, distributed energy resources, photovoltaics, machine learning, adaptive settings, estimation-based protection**

I. Introduction

In 2018, IEEE Standard 1547 was revised to, among other things, allow distributed energy resources (DER) to ride through voltage disturbances [1]. This important change would end any de facto reliance on undervoltage (UV) tripping as a method of fault detection for DER. Communication-based methods, e.g., direct transfer trip, can solve this protection issue but the cost presents a barrier to integration of distributed photovoltaics (PV). The system complexity also increases as the penetration level of PV increases, which causes the distribution system to resemble a meshed transmission system.

The Pacific Northwest National Laboratory is operated by Battelle for the U.S. Department of Energy under Contract DE-AC05-76RL01830. This material is based upon work supported by the U.S. Department of Energy's Office of Energy Efficiency and Renewable Energy (EERE) under the Solar Energy Technologies Office Agreement Number 34233. The views expressed herein do not necessarily represent the views of the U.S. Department of Energy or the United States Government.

The time overcurrent (TOC) protection schemes developed for radial distribution circuits don't apply to meshed systems. This project aimed to provide new fault detection methods that could work in the near term for circuits with high-penetration PV, emphasizing off-the-shelf or readily available equipment.

Fig. 1 shows the impact of recent changes to the default values and ranges for trip settings UV1 and UV2. Before 2018, DER were required to trip within 0.16 s after any applicable phase-phase or phase-neutral voltage fell below 0.5 pu. See the magenta shaded region in Fig. 1. For DER that doesn't contribute much fault current, e.g., PV, this UV2 function was often used to meet the functional requirements of detecting faults and unintentional islands. In 2014, an amendment allowed adjustment of the 0.16 s up to 1.0 s. The 2018 revision contains three disturbance-related categories of DER:

- Category I, the minimum, has the same default UV2 trip time of 0.16 s (the voltage setpoint is 0.45 pu). The UV2 time can be adjusted up to 2.0 s.
- Category II, which meets the needs of bulk system reliability, has the same UV2 default values and ranges as Category I. The difference is in a higher default time for UV1 to support ride-through of less severe voltage disturbances. The UV1 function is shaded in green in Fig. 1, but it's less relevant to detecting faults on the connected circuit.

- Category III, for high-penetration situations, has a default UV2 trip time of 2.0 s, with adjustability all the way up to 21.0 s.

Furthermore, the standard allows for adjustment of the UV1 and UV2 voltage setpoints, for any category, all the way down to 0.0 pu. If done, that would effectively remove the UV functions.

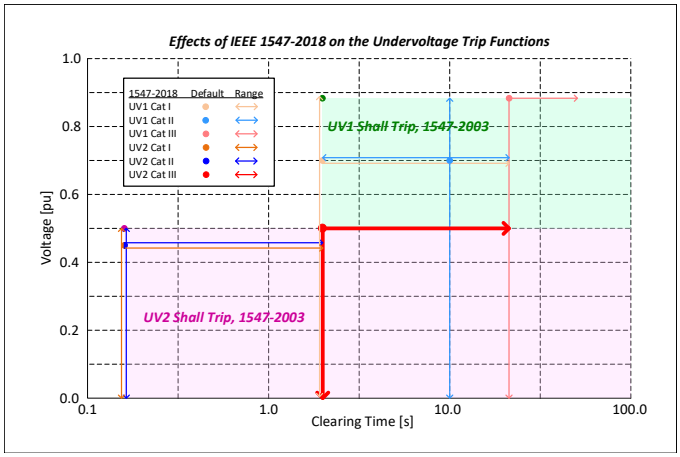

Fig. 1. IEEE 1547 revised undervoltage trip settings are less sensitive.

Inverter-based generation, including PV, doesn't contribute enough fault current for TOC protection schemes. Fig. 2 compares inverter-based and machine-based DER contributions (from one phase) to a nearby line-to-line fault (LLF). Before the fault at 0 cycles, the voltage and current is in phase for both. After the fault, the machine-based current increases to about 5 times rated, while the current angle shifts to lag the voltage. A Thevenin equivalent represents this behavior with a voltage source behind reactance. The inverter-based current increases much less, to approximately 1.15 pu of rated current in this example. At the fault instant, the current begins to lag the voltage, but is back in phase within two cycles. The inverter controls determine both behaviors, i.e, to maintain pre-fault power output within the inverter's capability, and to phase-lock the current and voltage waveforms. A Norton equivalent, with controlled current source, represents this behavior. Both magnitude and angle effects are important in protection system design.

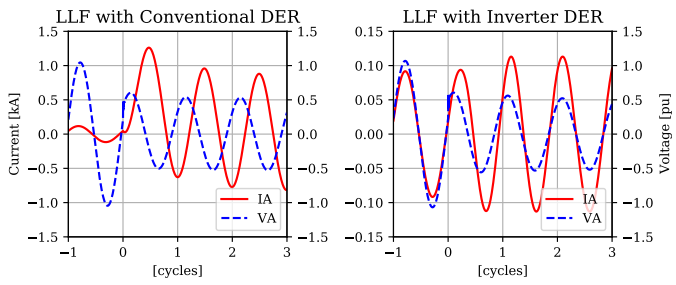

Fig. 2. Fault current from inverter-based DER (left) has lower magnitude and phase shift than from rotating machine DER (right).

The goal is to identify new protection schemes, not reliant on TOC and UV functions, that could work for scenarios of high-penetration DER. In an earlier project [2], we considered and ruled out some candidates:

- A single-point travelling wave scheme worked on simple feeder topologies. However, it wasn't robust to increasing numbers of lateral taps, distributed load connections (bushing capacitance, transformer, load), switching on capacitor banks, or multi-grounded neutral conductors.
- Focused directional overcurrent schemes work with rotating machines. However, PV doesn't contribute enough sustained current. Further, the interconnection transformer plays a dominant role if it provides a ground source.
- Negative sequence schemes were considered, but again, PV doesn't contribute enough sustained current. The controls are generally designed to suppress negative sequence current.

This paper considers distance schemes, which make use of both current and voltage measurements. These are more commonly found on transmission lines, but there have also been some distribution system applications [3]. References [4], [5] provide more information on accounting for taps and infeed on distribution circuits, while [6] contains some examples that are applicable to high-penetration DER. Given the time dependencies in Fig. 2, we also consider the incremental or time-domain distance schemes presented in [7] and [8].

A distance-based scheme could be implemented with off-the-shelf hardware. We also consider estimation-based [9] and learning-based schemes. Either of these could be implemented on real-time computing hardware, but with custom programming.

II. Tools and Methods

Table I summarizes characteristics of the test feeders we used to evaluate protection schemes. This paper will use results from the Electric Power Research Institute (EPRI) distributed photovoltaic (DPV) test feeder designated J1 [10]. The J1 feeder is based on a real utility feeder, with four commercial-scale PV sites (285, 190, 760 and 475 kW) and several residential sites. The IEEE 8500-node feeder has 1177 residential service transformers, providing candidate locations for rooftop residential PV. The other feeders have one or two sites for utility-scale PV. Results from feeders other than J1 will be discussed in [11].

Fig. 3 shows a notional feeder with one PV site, and several numbered protection zones bounded by circuit breakers and reclosers. Without PV, the utility devices rely on TOC coordiation. For example, during a fault on the main branch in zone 5, the immediate upstream recloser should trip first, while the feeder breaker provides backup via time delay. The PV site needs to trip in either case, otherwise the fault will not clear due to backfeed. In a dependable scheme, the PV site would trip for any fault in zones 4-7. In a selective scheme, the PV site would not trip for a fault in zones 1, 3, 8 or 9, unless the primary utility device failed to trip. In a

TABLE I
TEST FEEDER CHARACTERISTICS

Name	N_B	V	LD	PV	N_{PV}	N_R	N_F
DG Prot	10	12.47	1.0	1.65	1	3	20
Hull, MA	101	13.80	3.9	2.46	2	5	49
EPRI J1 [10]	3434	12.47	11.6	1.8	13	5	25
IEEE 8500	4876	12.47	12.9	0	1177	3	21
Utility 1	534	12.47	9.6	1.0	1	9	57
Utility 2	602	12.47	11.4	2.0	2	7	48
Utility 3	1093	34.50	27.6	20.0	1	15	42

N_B = number of buses; V = primary voltage [kV]
LD = peak load [MW]; PV = peak solar output [MW]
N_{PV} = number of photovoltaic sites
N_R = number of utility reclosers
N_F = number of fault type and bus combinations

secure scheme, the PV would not trip due to on-switching of the capacitor bank, which instantaneously looks like a short circuit. When the fault is in zone 2, the PV trips in 2-5 s to avoid unintentional islanding, or possibly faster if the feeder breaker fails to trip. We consider relays on the high-side of the interconnection transformer and the feeder breaker, indicated with green voltage transformer (VT) and current transformer (CT) symbols. Relay functions may also be incorporated into the reclosers. To evaluate a scheme's performance, we apply three-phase, single-line-to-ground (SLGF) and LLF at various locations and assess the fault clearing time, failures to trip, false trips, and most importantly, any uncleared faults.

Fig. 4 shows how models and data are used in the scheme evaluation. The feeder models from Table I were available in or converted to OpenDSS [12]. This tool is more commonly used for quasi-static time series power flow, at time steps down to 1 s, but it also performs dynamic phasor solutions at time steps down to 1 ms. We used this latter mode, with event-driven relay models of TOC, UV and overvoltage (OV) trip functions built into the tool. Waveform data is created with electromagnetic transient (EMT) simulation. We chose the Alternative Transients Program (ATP) [13] because it worked with Python scripts converting OpenDSS models to ATP models, see Fig. 4. ATP is able to produce waveform data in a standard format [14], which fed a Python model of the relay function under consideration, and also drove the physical relays in open-loop laboratory testing. Relays in the field also collected waveform data in the same standard format for event analysis.

The existing tools, OpenDSS and ATP, lacked models of the DER fault behavior. To address this gap, three-phase and single-phase inverter models from [15] were implemented to control power output during a fault, suppress negative sequence current, and simulate the phase-locked loop. The ATP implementation is available at [16] to licensed ATP users, while the OpenDSS implementation is available at [17]. Both models are parameterizable to some extent, but vendor-specific models would yield more accurate results.

The existing tools also lacked incremental distance relay functions, and in the case of OpenDSS, regular distance relay functions. A rectangular distance relay function was added to OpenDSS [18], along with one of the incremental distance functions from literature [7]. These operate in phasor-dynamic simulation. A waveform incremental distance relay function was implemented in Python, based on the information publicly available in [8], [19], [20].

The public models and code will be made available under an open source license [21]. This will not include the script converting OpenDSS to ATP models, because of ATP licensing requirements. The script performs optional model order reduction, and then converts lines, transformers, loads and capacitor banks from OpenDSS to ATP. The user still has to add PV and other components manually. Researchers who are interested in this conversion script may post a request to the ATP mailing list, and the project team may be able to respond.

III. DISTANCE PROTECTION

Fig. 5 shows a footprint of the J1 feeder solved at peak load in OpenDS, with 3434 buses. Fig. 6 shows the reduced-order J1 model with 74 buses, used in the ATP and phasor-dynamic simulations. Only the four largest PV sites are highlighted in the reduced-order model; they will have distance or other advanced relays. The retained buses were chosen manually to include protection zone boundaries, extreme ends of the feeder, major junction points, capacitor banks and PV sites. Both tools can run the full-order model, but the reduced-order model is more efficient for iterative and exploratory work. To check selectivity, three external fault locations were added to a parallel feeder that is not part of the original J1 model. These locations, highlighted in red, are 300 ft, 1 mile and 2 miles out from the substation.

Table II summarizes distance relay function settings for the utility devices and four PV sites on J1. These utility device settings implement single overreaching zones, coordinated by the time delay, Dly. A real implementation might use two or three zones, as in transmission systems. The setting angles are lower than on transmission lines. For the incremental distance function, a supervisory overcurrent threshold, I_{OC}, must be used. Helper scripts to determine the utility device settings are at [21].

TABLE II
J1 FEEDER DISTANCE RELAY SETTINGS

Device	Z_{1mag}	Z_{1ang}	Z_{0mag}	Z_{0ang}	Dly	I_{OC}
Fdr	4.27	49.58	6.67	56.37	0.19	300.0
A	4.06	43.99	2.64	15.50	0.12	250.0
B[a]	9.84	35.29	5.77	19.68	0.01	250.0
C	8.17	40.60	7.88	42.57	0.07	150.0
D	9.15	42.11	5.92	34.46	0.01	150.0
PV1	70.00	10.00	70.00	10.00	0.50	101.0
PV2	100.00	10.00	100.00	10.00	0.50	68.0
PV3	30.00	10.00	30.00	10.00	0.50	220.0
PV4	250.00	10.00	250.00	10.00	0.50	24.0

Z_{1mag}, Z_{1ang} = positive sequence primary reach [Ω], [deg]
Z_{0mag}, Z_{0ang} = zero sequence primary reach [Ω], [deg]
Dly = trip time delay [s]
I_{OC} = overcurrent supervision threshold [A]
[a]Multiply Z_{1mag} and Z_{0mag} by 1.5 for incremental distance.

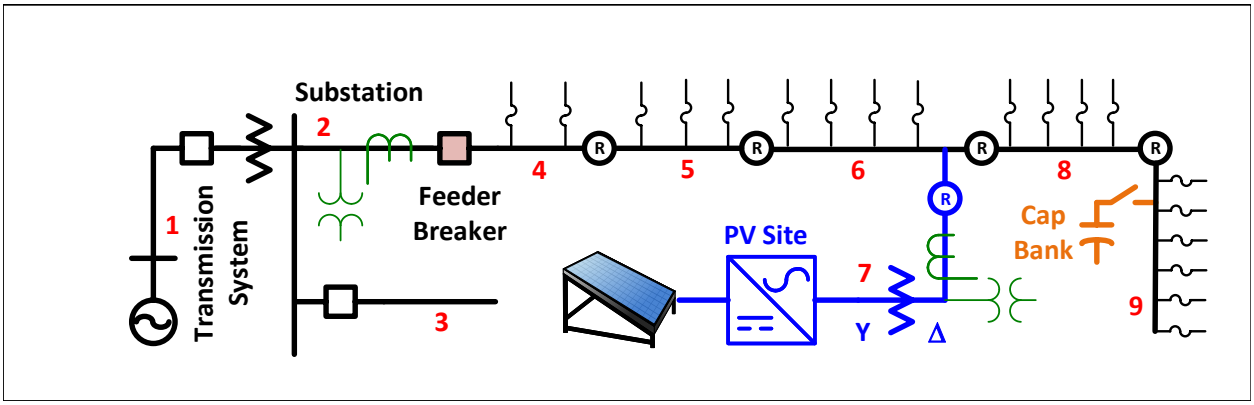

Fig. 3. Feeder with one PV site, one capacitor bank and nine protection zones defined by breakers and reclosers.

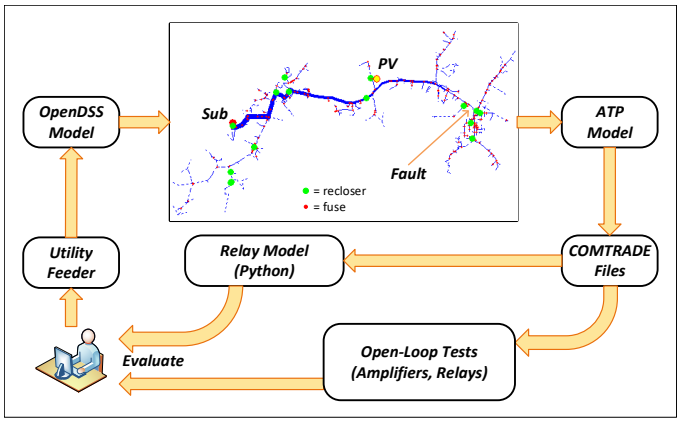

Fig. 4. Relay analysis uses EMT simulation and open-loop hardware tests.

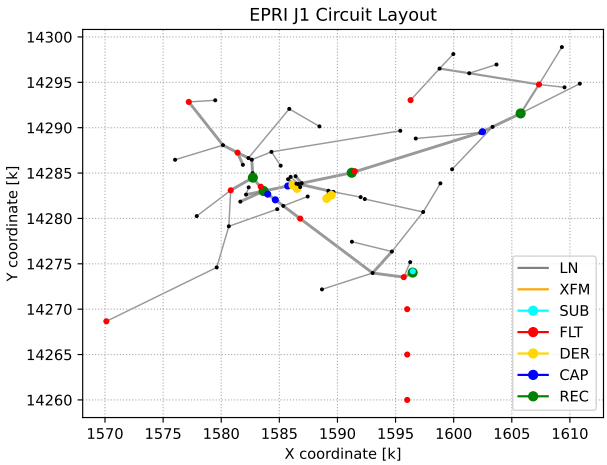

Fig. 6. EPRI J1 feeder model reduced for ATP simulation.

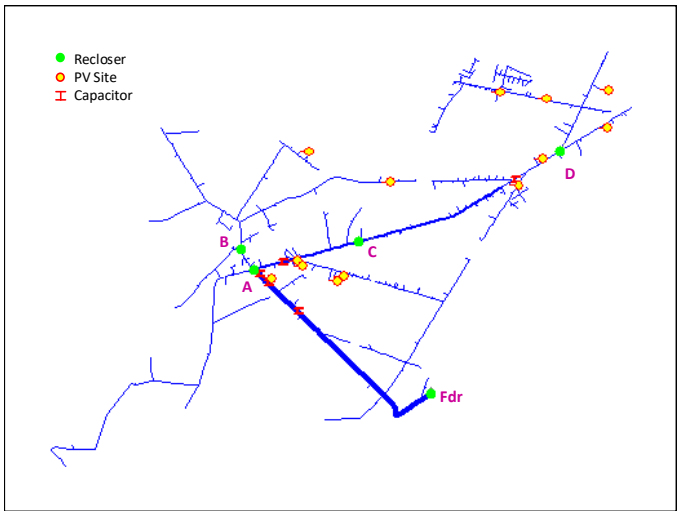

Fig. 5. EPRI DPV J1 feeder power flow solution in OpenDSS.

The PV functions are set following a different principle, as the inverter controls influence PV voltage and current. In Table II, the PV sizes were increased by a factor of seven to represent 105% penetration of PV with respect to feeder peak load. These higher sizes determine I_{OC} values. In turn, the PV setting magnitudes are below the ratio of phase-neutral voltage, 7200, divided by I_{OC}. Instead of tripping on sub-cycle transients, the Table II settings will trip on the in-phase ratio of voltage and current, relying on Dly to mitigate false trips. When a fault occurs, if the utility devices trip first, the PV devices will be able trip on the distance or (better) the incremental distance function. Both distance and incremental distance functions use the same settings, except as noted for recloser B, and that only incremental distance uses I_{OC}.

Fig. 7 shows the fault current and feeder breaker (Fdr) response to a SLGF on phase B within the first protective zone, between Fdr and recloser A. At 0.1 s, the fault initiates and the fault current exceeds 4 kA. The Fdr trips after 0.324 s and its current drops to zero, but the fault is still fed by the PV sites, and it does not clear until after 0.668 s. Fig. 8 shows

the PV interconnection transformer primary currents on phase B during the event. The exponential time constants are due to model initialization at time zero, and later on they are caused the fault and other switching events. The largest inverter, PV3, trips after Fdr at about 0.468 s, followed by the other three inverters after 0.632 s. At this point, the fault has been cleared.

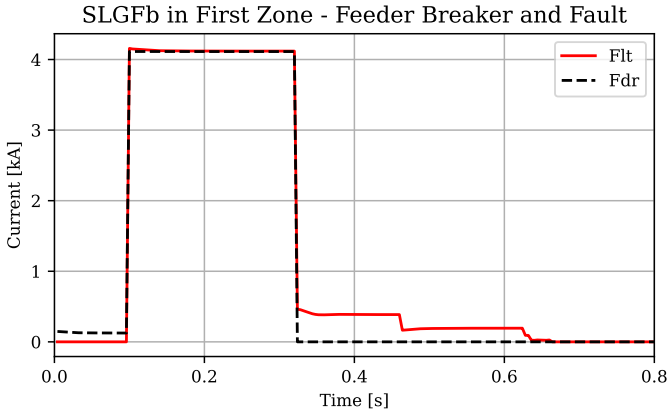

Fig. 7. EPRI J1 ground fault in first zone; fault and feeder currents.

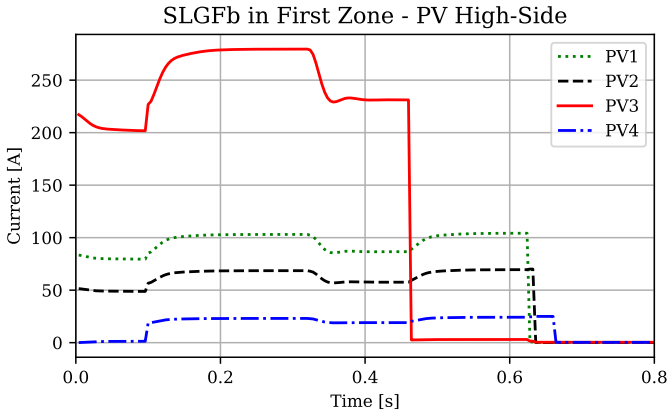

Fig. 8. EPRI J1 ground fault in first zone; PV transformer currents.

Table III compares the performance of TOC, distance and incremental distance schemes at 105% penetration of distributed PV, i.e., the PV capacity exceeds feeder peak load by 5%. At this level, reverse power flow through the substation would be expected several hours per day. In the first three rows, all utility devices use TOC functions and the PV sites rely on UV2 with settings:

- Cat I: 0.45 pu, 0.16 s
- Cat II: 0.45 pu, 2.00 s
- Cat III: 0.10 pu, 21.00 s

The last two rows, representing distance and incremental distance, retain the UV2 functions as required by IEEE Std 1547-2018. However, the utility devices use a distance or incremental distance function instead of TOC, and the PV sites add the distance or incremental distance function. There are no instances of uncleared faults, N_U, or of the utility device failing to trip, N_{FL}. There are many instances of utility recloser false trips or overtripping, N_{FS}, which interrupt more customers than necessary to clear the fault. Automatic reclosing would restore service to those customers. With TOC the time to clear, T_C, is especially high using Category III. At higher penetration level, when utility devices open to isolate PV with some of the load, the PV relies on UV2, or an overvoltage trip function, to clear the fault.

In a Pareto sense, the distance and incremental distance functions perform better than TOC at Category III. The PV tripping dependability needs to improve, which would improve T_C even further.

TABLE III
J1 FEEDER RELAY SCHEME PERFORMANCE AT 105% PENETRATION

Scheme	N_U	N_{FL}	N_{FS}	T_C
Time Overcurrent Cat I	0	0	12	0.099
Time Overcurrent Cat II	0	0	27	0.522
Time Overcurrent Cat III	0	0	28	4.846
Distance Cat III	0	0	11	3.356
Incremental Distance Cat III	0	0	21	3.010

N_U = number of uncleared faults
N_{FL} = number of failed utility recloser trips
N_{FS} = number of false utility recloser trips
T_C = mean clearing time of cleared faults [s]

IV. ESTIMATION-BASED PROTECTION

The basic idea of the setting-less protection relay, Fig. 9 has been inspired by the differential protection function (no coordination needed), with some differences. In differential protection, the electric currents at all terminals of a protection zone are measured, and their weighted sum must be equal to zero according to a generalized Kirchhoff's current law (KCL). As long as the sum is zero or near zero, no action is taken. In estimation-based protection (EBP), all available measurements within the protection zone and at its boundaries are utilized. When there is no fault within the protection zone, the measurements should satisfy the dynamic model of the protection zone. If not, a trip signal is generated.

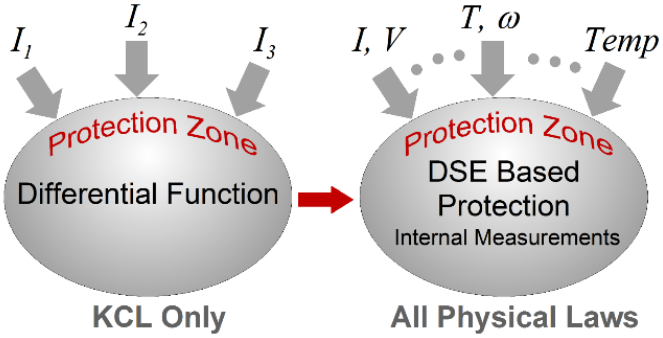

Fig. 9. Settingless relay applies measurements to mathematical model.

In Fig. 10, the distribution circuit protection zone is not fully observable because the tapped loads, and perhaps some of the smaller DER are not measured. This was expected to be

a challenge in applying the method to high-penetration DER. The process is mathematically formulated as a dynamic state estimation, which provides a quantitative assessment of how well the measurements of the zone fit its dynamic model in real time. A preferred implementation is to use merging units to obtain measurements which are streamed to the setting-less relay through a process bus. The dynamic state estimation computes the best estimate of the protection zone states. It also computes the goodness of fit, or the probability that the measurements fit the zone model, within the accuracy of the metering used via chi-square test. A low probability indicates abnormalities/faults in the protection zone. The chi-square test typically returns a probability of 100% for healthy protection zones and 0% for a protection zone with any type of internal fault.

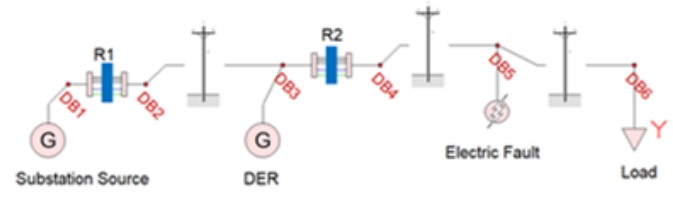

Fig. 10. DER integrated into a zone for estimation-based protection.

An example of application of an EBP relay is shown in Fig. 11. The protection zone is a section of a distribution line belonging to one of the partner utilities, with model order reduction as described earlier.

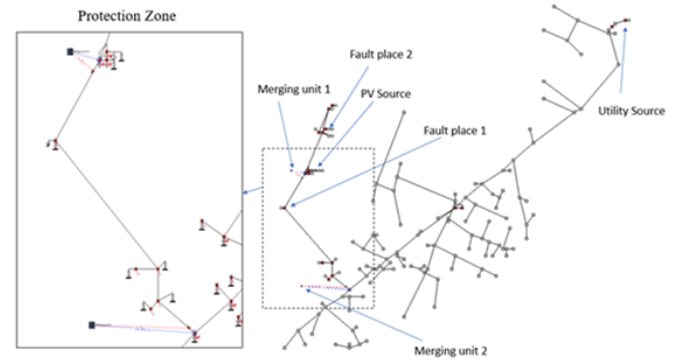

Fig. 11. Utility circuit modeled for estimation-based protection.

Fig. 12 illustrates a simulation of two successive faults and the response of the EBP. The first fault is an internal fault and initiates at time 0.429 s. The second fault is outside the protection zone and initiates at 0.938 s. Each of the faults persist for 0.215 seconds. For brevity we show the voltage and currents at the two ends of the distribution line section of the faulted phase only. During the external fault, the voltage magnitude is lower and the current magnitude is higher than for the internal fault. The bottom three traces (5, 6 and 7) show part of the computations from the dynamic state estimation. Trace 5 shows the computed chi-square, i.e. the sum of the residuals squared. Only during the internal fault is this quantity substantially higher than zero, indicating a difference between the model of the protection zone and the measurements. Trace 6 is the probability that the measurements are consistent with the model of the protection zone within the accuracy of the measurements. It goes to zero only during the internal fault and it is 1.0 for the rest of the time, except with one short burst during a transient around time 1.152 sec. Finally, trace 7 provides the trip signal. Reference [22] describes the EBP results in more detail.

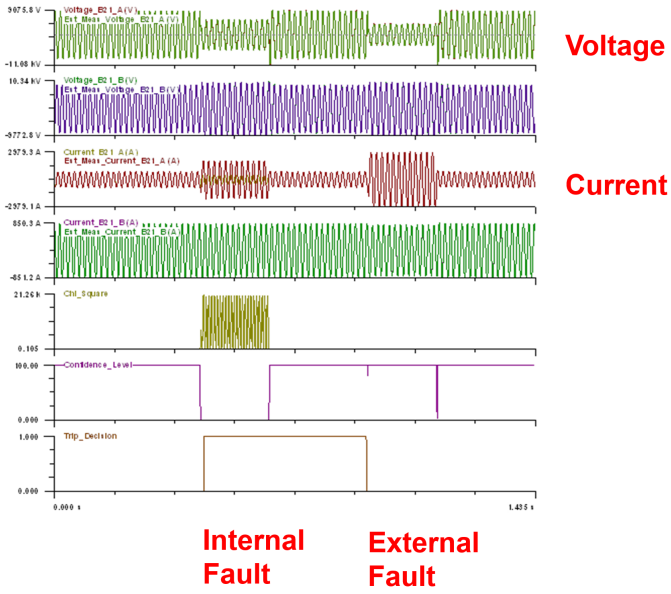

Fig. 12. Estimation-based relay distinguishing fault zones even with incomplete measurements.

V. Learning-Based Protection

The convolutional neural network (CNN) scheme is entirely a data-driven relay. As shown in Fig. 13, it attempts to identify the fault just from local current and voltage waveforms. In Fig. 13 those waveforms might be recognized as a capacitor switching transient. The CNN attempts to identify fault zones based on the images of waveforms. In this project, training and testing waveforms were created by ATP simulation, with the equivalent of a 10-kHz sampling rate. The trained model of CNN could be downloaded to the relay, implemented in a real-time automation controller (RTAC). The CNN training requires an EMT model of the distribution system. It could be updated after installation from real-time data. In preliminary work with a 34-bus public test system, the overall accuracy was 99.88%, with 0.29% false positives and no false negatives. However, this only distinguished between faults, load switching and capacitor switching. Multiple protection zones and parallel feeders were not included.

Fig. 14 shows the CNN structure used here. We chose CNN with rectified linear activation units (ReLU) because of their success with image classification, feature extraction and feature recognition, which are similar tasks to fault classification. With reference to Fig. 6, there are five internal

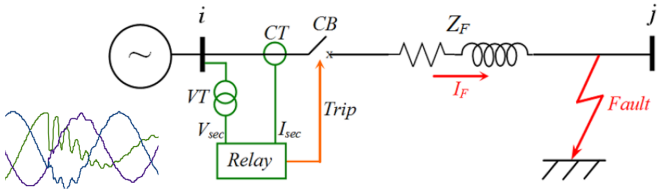

Fig. 13. Data-driven relay learning from local measurements.

protection zones numbered 0 to 4 for devices C, D, B, A, and Fdr, respectively. The external fault zone is number 5 and the capacitor switching zone is number 6, for seven possible event outcomes. The output layer in Fig. 14 provides a probability estimate for each outcome.

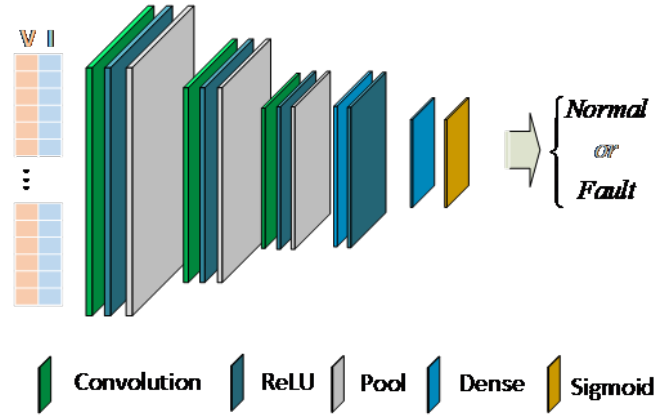

Fig. 14. Learning relay architecture for fault zone identification.

The three-phase voltages and currents are measured on the high side of transformer at PV3, the largest DER installation rated 760 kW. These six waveforms are vertically stacked. 1000 events are simulated and labelled for each protection zone, with 80% used for training and 20% retained for testing. Adam optimization is used for the training with categorical cross entropy as the loss function. Prediction accuracy is measured as the performance metric. Samples are randomly shuffled in the input data set. Cross-validation is used to evaluate different CNN architectures. The model is trained for 20-25 epochs with a batch size of 64 samples. 20% of training data is used for cross-validation. 1-D convolutional layers with a kernel size of 3 and stride length of 1 are used. Max pooling is used to down sample the image, with every alternate convolutional layer. The convolutional layers are connected to fully connected network. For better generalization a dropout of 0.35 is used. All the layers except the final layer uses the relu activation. The output layer uses the softmax activation with outputs equal to number of protection zones. The output layer gives a prediction of the probability density of a given fault occurring in various protection zones. The region with a maximum probability is used as a predicted target value. Fig. 15 and 16 show that the training and validation metrics converge within ten to fifteen epochs.

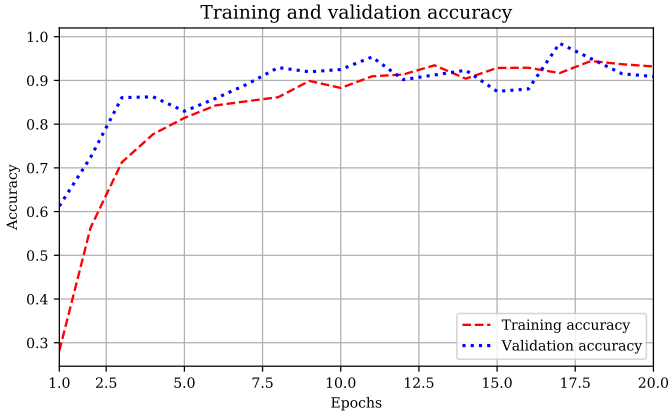

Fig. 15. Training and validation accuracy for J1 learning relay.

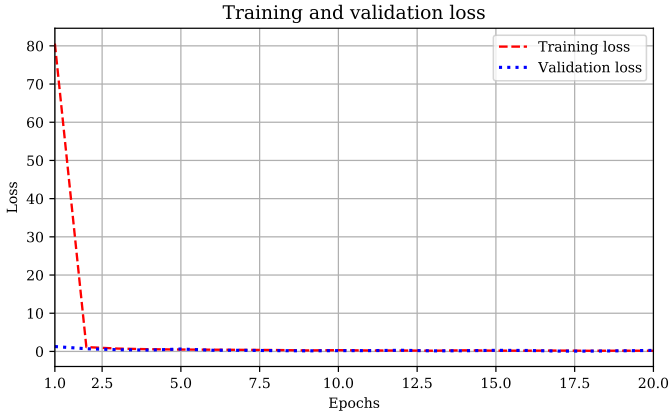

Fig. 16. Training and validation loss for J1 learning relay.

Fig. 17 displays the confusion matrix for one of the relays. With 20% of 1000 events retained for testing, a perfect result would have values of about 200 in each diagonal element, and zeros in every off diagonal element. Where non-zero entries occur, the fault zone was not properly identified. These identification errors don't all have the same consequence. For example, there were 31 faults in zone 1 that were incorrectly identified in zone 0, and 7 faults in zone 0 that were misidentified in zone 1. These are the zones downstream of reclosers C and D. Unless those reclosers fail to clear the fault, PV3 should not trip for either zone 0 or zone 1. Furthermore, there were 9 events from zone 5 erroneously identified to zone 6, but PV3 should not trip for either one. The consequential identification errors are:

- One case of predicted zone 2 (B) vs. actual zone 4 (Fdr). PV3 would fail to trip when it should, representing a false negative rate of 1/207 or 0.48%.
- One case of predicted zone 6 (capacitors) vs. actual zone 3 (A). PV3 would fail to trip when it should, representing a false negative rate of 1/202 or 0.49%

The overall testing accuracy exceeds 95%. Improvements could be made with additional training or by adjusting some zone boundaries; see [11] for more details.

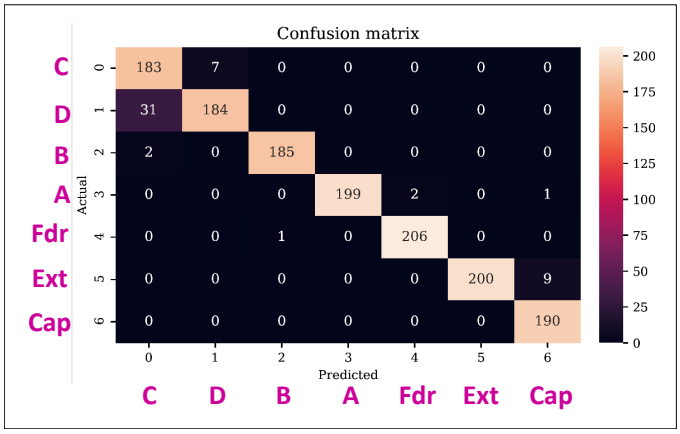

Fig. 17. Confusion matrix of actual and predicted fault zones.

VI. Conclusions

This project has identified some promising schemes that could supplant the reliance on UV trip functions to detect faults in high-penetration PV scenarios:

- Distance relays could take the place of utility TOC devices. These functions are also useful at the PV sites, but not necessarily dependable enough for production use in this application. The UV2 trip function should be retained, even if at 0.10-pu voltage and 21-s time delay, for dependability.
- Estimation-based protection and learning-based protection have shown promising results. Both of them require a more detailed model and simulation platform than traditional TOC schemes.

With inverter-based resources and new protection schemes entering the picture, accurate EMT models and simulations will become more important. This project has developed some test systems and tools for public use, with others that may be available to licensed ATP users. Waveform data collection continues at the utility partner sites, for use in follow-up research projects. This waveform data may help inform the consideration of changes in inverter fault response, e.g., the injection of negative sequence current as a relaying quantity.

References

[1] *IEEE Standard for Interconnection and Interoperability of Distributed Energy Resources with Associated Electric Power Systems Interfaces*, IEEE Std 1547-2018.

[2] T. E. McDermott, R. Fan, P. Thekkumparambath Mana, B. GNVSR Vyakaranam, T. Smith, J. Hambrick, Z. Li, and A. Barnes, "Relaying for distribution and microgrids evolving from radial to bidirectional power flow", 2019, doi: 10.2172/1574999.

[3] A. Sinclair, D. Finney, D. Martin and P. Sharma, "Distance protection in distribution systems: how it assists With integrating distributed resources," in *IEEE Trans. Industry Applications*, 2014, doi: 10.1109/TIA.2013.2288426.

[4] V. C. Nikolaidis, C. Arsenopoulos, A. S. Safigianni and C. D. Vournas, "A distance based protection scheme for distribution systems with distributed generators," in *2016 PSCC*, 2016, doi: 10.1109/PSCC.2016.7541019.

[5] J. Ma, W. Ma, Y. Qiu and J. S. Thorp, "An adaptive distance protection scheme based on the voltage drop equation," in *IEEE Trans. Power Delivery*, 2015, doi: 10.1109/TPWRD.2015.2404951.

[6] A. Hooshyar and R. Iravani, "Microgrid protection," in *Proc. IEEE*, 2017, doi: 10.1109/JPROC.2017.2669342.

[7] C. Dzienis, M. Kereit, and J. Blumschein, "Analysis of high-speed-distance protection", in *Intl. Conf. Adv. Power Sys. Automation and Protection*, 2011, doi: 10.1109/APAP.2011.6180585.

[8] E. O. Schweitzer and B. Kasztenny, "Distance protection: Why have we started with a circle, does it matter, and what else is out there?", in *CPRE*, 2018, doi: 10.1109/CPRE.2018.8349791.

[9] A. P. S. Meliopoulos, G. J. Cokkinides, P. Myrda, Y. Liu, R. Fan, L. Sun, R. Huang, and Z. Tan, "Dynamic state estimation-based protection: status and promise," in *IEEE Trans. Power Delivery*, 2017, doi: 10.1109/TPWRD.2016.2613411.

[10] EPRI, "Feeder j1", 2010, [Online]. Available: https://dpv.epri.com/feeder_j.html

[11] T. E. McDermott, N. E. Shepard, A. P. S. Meliopoulos, M. Ramesh, J. D. Doty, and J. T. Kolln, "Protection of distribution circuits with high penetration of solar pv", PNNL, 2021, to be published [Online]. Available: https://www.osti.gov/

[12] R. C. Dugan and T. E. McDermott, "An open source platform for collaborating on smart grid research," in *2011 IEEE PES General Meeting*, 2011, doi: 10.1109/PES.2011.6039829.

[13] European EMTP-ATP Users Group, *Alternative Transients Program (ATP)*, 2018 [Online]. Available: https://www.emtp.org/

[14] *IEEE/IEC Measuring relays and protection equipment – Part 24: Common format for transient data exchange (COMTRADE) for power systems*, IEEE Std C37.111-2013.

[15] R. Teodorescu, M. Liserre, and P. Rodriguez, *Grid Converters for Photovoltaic Systems*, Wiley-IEEE, 2011.

[16] T. E. McDermott, "Testpll case 92", 2019, [Online]. Available: http://www.atpdraw.net/cases.php

[17] T. E. McDermott, "Opendss technical note: Voltage-controlled current source", 2021, [Online]. Available: https://sourceforge.net/p/electricdss/code/HEAD/tree/trunk/Distrib/Doc/Voltage-Controlled-Current-Source.pdf

[18] T. E. McDermott, "Opendss technical note: Distance relays", 2021 [Online]. Available: https://sourceforge.net/p/electricdss/code/HEAD/tree/trunk/Distrib/Doc/Distance_Relays.pdf

[19] E. O. Schweitzer, B. Kasztenny, A. Guzman, V. Skendzic, M. Mynam, "Speed of line protection – can we break free of phasor limitations?", in *CPRE*, 2015, doi: 10.1109/CPRE.2015.7102184.

[20] E. O. Schweitzer, B. Kasztenny, and M. V. Mynam, "Performance of time-domain line protection elements on real-world faults," in *CPRE*, 2016, doi: 10.1109/CPRE.2016.7914904.

[21] "Distributed PV Protection Code", 2021, to be published [Online]. Available: https://github.com/pnnl/dpv-prot/

[22] A. P. S. Meliopoulos and G. J. Cokkinides, "Estimation based protection relay-application to distribution system with high der penetration", Georgia Tech, 2020, to be published [Online]. Available: https://www.osti.gov/